JOURNAL OF AIRCRAFT
Vol. 40, No. 1, January–February 2003

Dynamic Stall Alleviation Using a Deformable Leading Edge Concept—A Numerical Study

Mehmet Sahin* and Lakshmi N. Sankar†
Georgia Institute of Technology, Atlanta, Georgia 30332-0150
M. S. Chandrasekhara‡
Naval Postgraduate School, Monterey, California 93943
and
Chee Tung§
NASA Ames Research Center, Moffett Field, California 94035-1000

Dynamic stall calculations were carried out for an airfoil with a dynamically deformed leading-edge (DDLE) shape at a freestream Mach number of 0.3. The surface deformations were done about a baseline NACA 0012 airfoil, effectively increasing the airfoil leading-edge radius and thickness at high angles of attack. It was found that the DDLE airfoil had a slightly dynamic stall behavior compared to the baseline NACA 0012 airfoil. In particular, the lift, drag, and pitching-moment hysteresis loops were milder for the DDLE airfoil compared to the baseline airfoil. It was also found that a static shape that corresponds to the thickest deformed shape performed just as well as the DDLE shape, indicating that the shape itself, and not its time rate of change, was the reason for the improved performance. At higher Mach numbers around 0.4, the DDLE shape exhibited a strong dynamic stall triggered by a shock-induced separation, offsetting any benefit from the change in the shape of the airfoil. Additional work is needed on the development of DDLE shapes that will perform well at higher speeds.

Introduction

ROTARY-wing aircraft often experience a dynamic stall phenomenon over the retreating blade. Three types of stall—light stall, moderate stall, and strong dynamic stall—have been observed in literature.[1] The strong dynamic stall phenomenon involves three phases. The lift initially increases as the airfoil pitches up and continues to increase well past the static stall value $C_{l,\max}$. Toward the end of the upstroke, a vortex begins to form near the leading edge and grows in strength. Toward the beginning of the downstroke, or shortly thereafter, this vortex is shed from the upper surface, creating a rapid loss in the bound circulation and lift. As this vortex rolls downstream over the upper surface, it causes large reductions in local pressure and high nose-down pitching moments. As the airfoil pitches down, one or more weaker vortices are shed from the upper surface, creating additional fluctuations in lift and pitching moment. The flow eventually reattaches at lower angles of attack.

The pitching moments, along with its large variations, are transferred to the vehicle through pitch links or a flex beam. These components may fail as a result of the high cycle fatigue that develops. These loads also cause vibrations of the fuselage, passenger discomfort, and structural fatigue. Many electronic components and systems (e.g., chips mounted on boards) may experience random failures if the g loads are high enough and frequent enough to unseat them.

Many dynamic stall load-alleviation concepts have been proposed in literature. Carr and McAlister[2] proposed a leading-edge slat device, which operates much like a slat on a wing and suppresses the leading-edge stall. Tuncer and Sankar[3] have numerically studied this using a two-dimensional multielement dynamic stall solver. A limited number of three-dimensional calculations have also been done by Bangalore and Sankar[4] to demonstrate that leading-edge slats are effective in alleviating dynamic stall. The major drawback of slats is the high drag penalty associated with their use at off-design conditions. A retraction mechanism similar to that found on aircraft will be heavy and costly. For these reasons this device has not been pursued by the industries.

Another concept that is gaining wide attention is the "synthetic jet" concept. In this approach mass-less jets generated by flexible cavity walls are used to alter the boundary-layer behavior and prevent stall.[5] If the jets are strong enough, they can act as spoilers destroying lift or as vortex flaps increasing lift. The ability of synthetic jets to eliminate undesirable loads and pitching moments has been computationally studied by Hassan at Boeing Mesa.[6]

A third concept for dynamic stall alleviation is the "dynamically deforming leading-edge (DDLE)" concept proposed by Chandrasekhara and Carr.[7] In this approach the airfoil shape is gradually changed, and the leading-edge radius is increased as the airfoil pitches up. Airfoils with large leading-edge radii tend to have mild adverse pressure gradients because the peak local velocities are lower than that for a conventional airfoil. As the airfoil pitches down and there is no danger of stall, the airfoil returns to its original shape.

In this work the DDLE concept is computationally studied. A two-dimensional compressible Navier–Stokes solver is modified to handle arbitrary moving boundaries for the given time schedule. The baseline shape is a NACA 0012 airfoil, which is deformed according to the schedule prescribed in Ref. 6. It is demonstrated that the dynamic stall process is indeed alleviated by the use of the deforming leading-edge shape. This is done through a comparison of the surface-pressure distributions and load hysteresis loops for the baseline NACA 0012 airfoil and the DDLE airfoil.

Presented as Paper 2000-0520 at the 38th Aerospace Science Meeting and Exhibit, Reno, NV, 10–13 January 2000; received 30 August 2000; revision received 21 May 2001; accepted for publication 21 May 2001.

*Graduate Research Assistant, School of Aerospace Engineering. Student Member AIAA.
†Regents' Professor, School of Aerospace Engineering. Associate Fellow AIAA.
‡Research Professor and Associate Director, Department of Aeronautics and Astronautics. Associate Fellow AIAA.
§Research Scientist, Army/NASA Rotorcraft Division, Aerodynamics Directorate (AMRDEC), AMCOM. Associate Fellow AIAA.

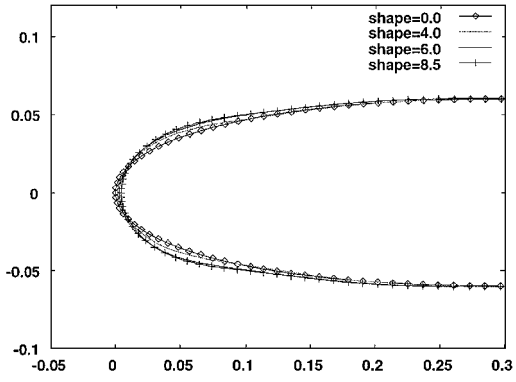

Fig. 1 DDLE airfoil shape profiles.

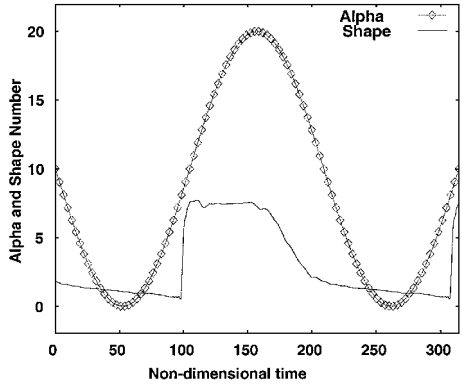

Fig. 2 DDLE shape and angle-of-attack history (V1V05SO-8D5).

Mathematical and Numerical Formulation

A two-dimensional compressible Navier–Stokes solver is used in this study. This solver uses a curvilinear body-fitted grid that will pitch up or down with the airfoil. The scheme is second-order or fourth-order accurate in space and is first-order accurate in time. A two-layer eddy viscosity model is used to account for the effects of turbulence. Wu and Sankar describe the mathematical formulation behind this analysis and applications of this solver.[8] Three-dimensional versions of this solver that can model oscillating wings[9] and rotors also exist.[10]

At each time step the airfoil surface and the surrounding grid are distorted using the schedule provided in Ref. 6. For the given discrete set of airfoil surface points, the Gram–Schmidt orthonormalization process described in Ref. 11 is used to generate a smooth function defining the airfoil geometry. The dynamic grid adaptation used here is similar to the work of Batina.[12] The grid around the body is considered to be a system of interconnected springs. This system is constructed by representing a grid line joining two successive grid points by a tension spring. Whenever the airfoil boundary moves, all of the grid nodes must be adjusted so that the nodes are force free.

The value of spring stiffness determines how much a node will move and can be specified in different ways. In this work the spring stiffness is assumed inversely proportional to length of distance between two successive grid points and given as

$$k_{m,k} = 1.0 \Big/ \left[(x_{m,k} - x_{i,j})^2 + (y_{m,k} - y_{i,j})^2 \right]^{p/2} \tag{1}$$

where p is a parameter used to control the stiffness of the spring (chosen as 5). The grid deformation as a result of boundary geometry change is solved explicitly by using several Jacobi iterations:

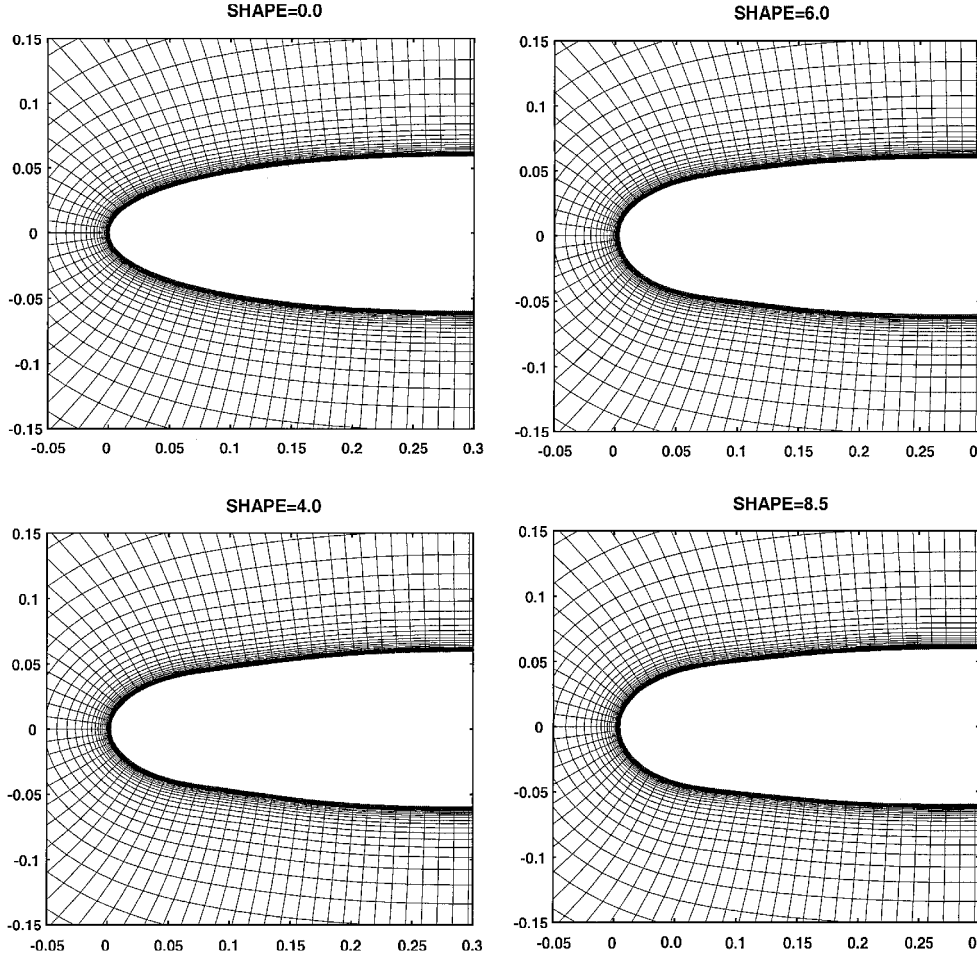

Fig. 3 Leading-edge grid deformation for DDLE airfoil shape profiles.

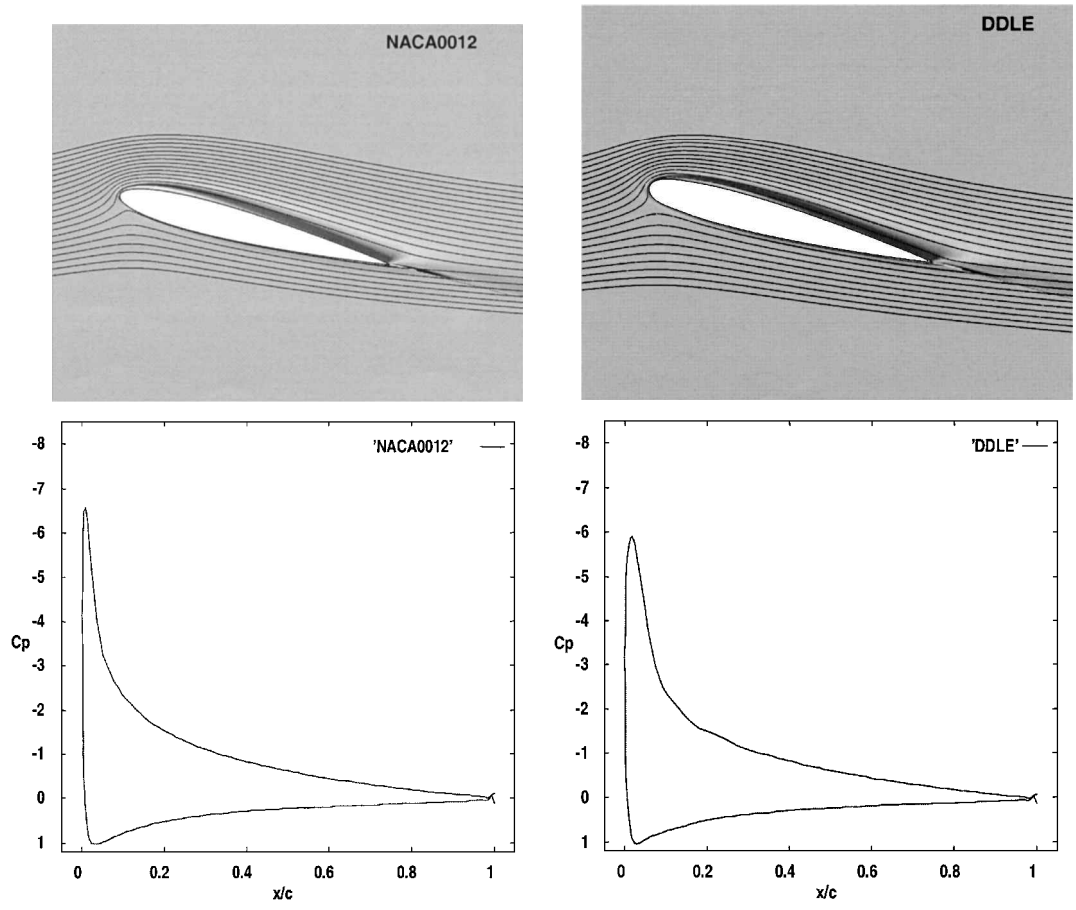

Fig. 4a Streamlines, vorticity contours, and surface-pressure coefficient over the NACA 0012 airfoil at α = 14.62 deg.

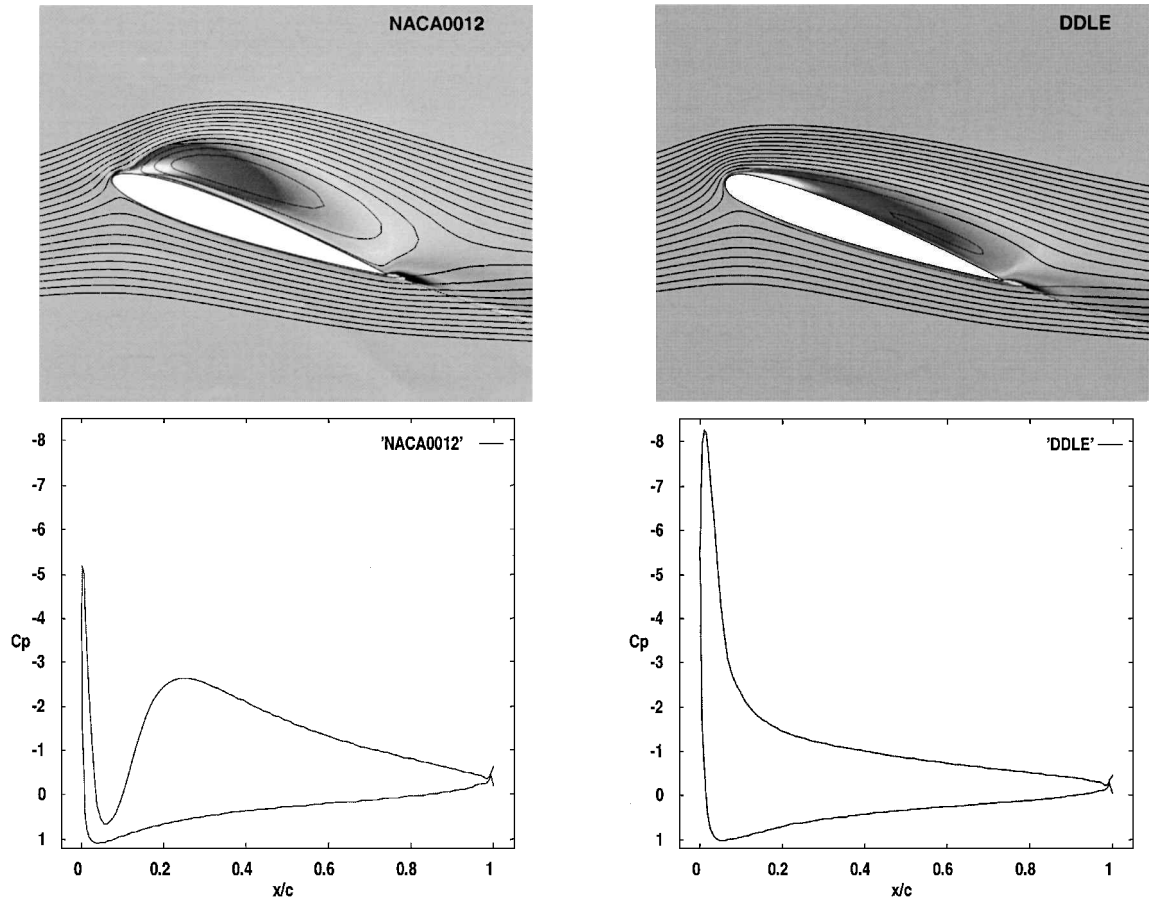

Fig. 4b Streamlines, vorticity contours, and surface-pressure coefficient over the NACA 0012 airfoil at α = 19.43 deg.

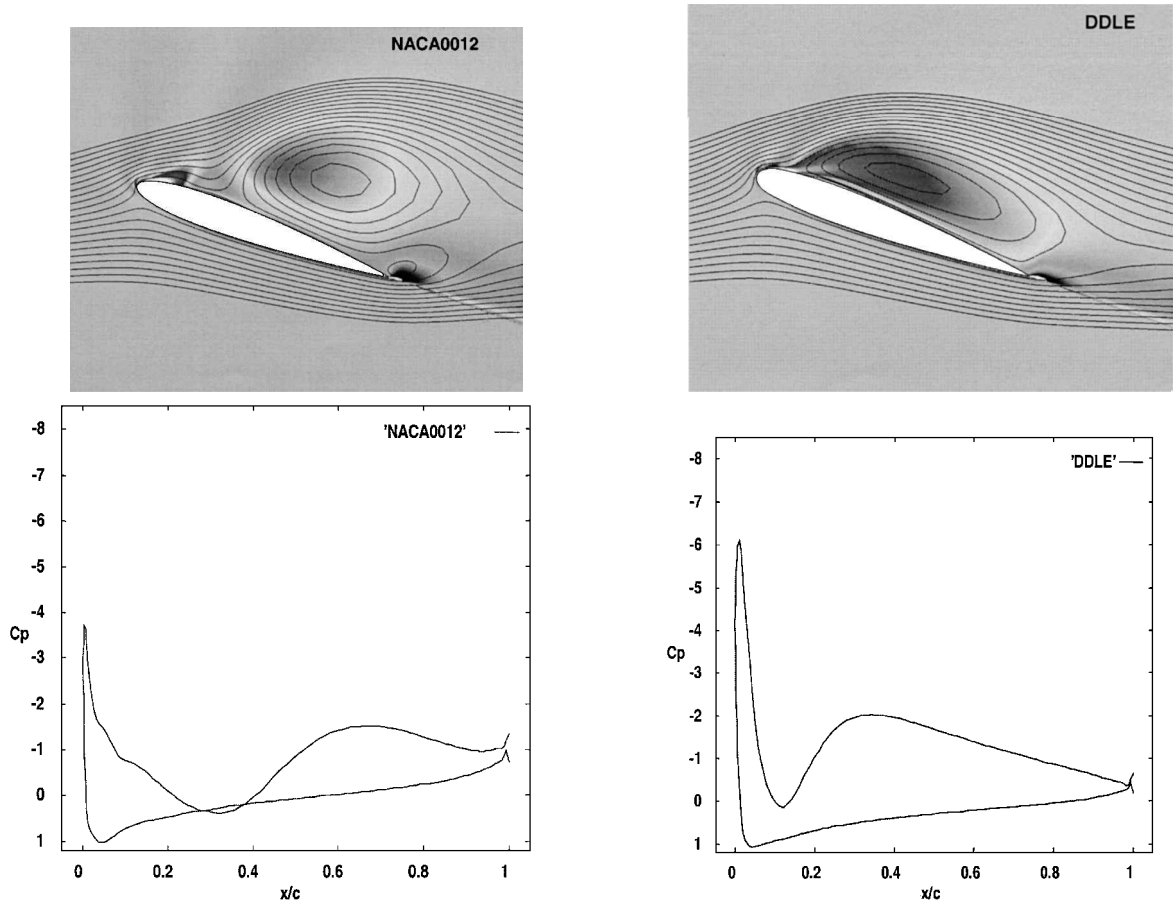

Fig. 4c Streamlines, vorticity contours, and surface-pressure coefficient over the NACA 0012 airfoil at α = 20.00 deg.

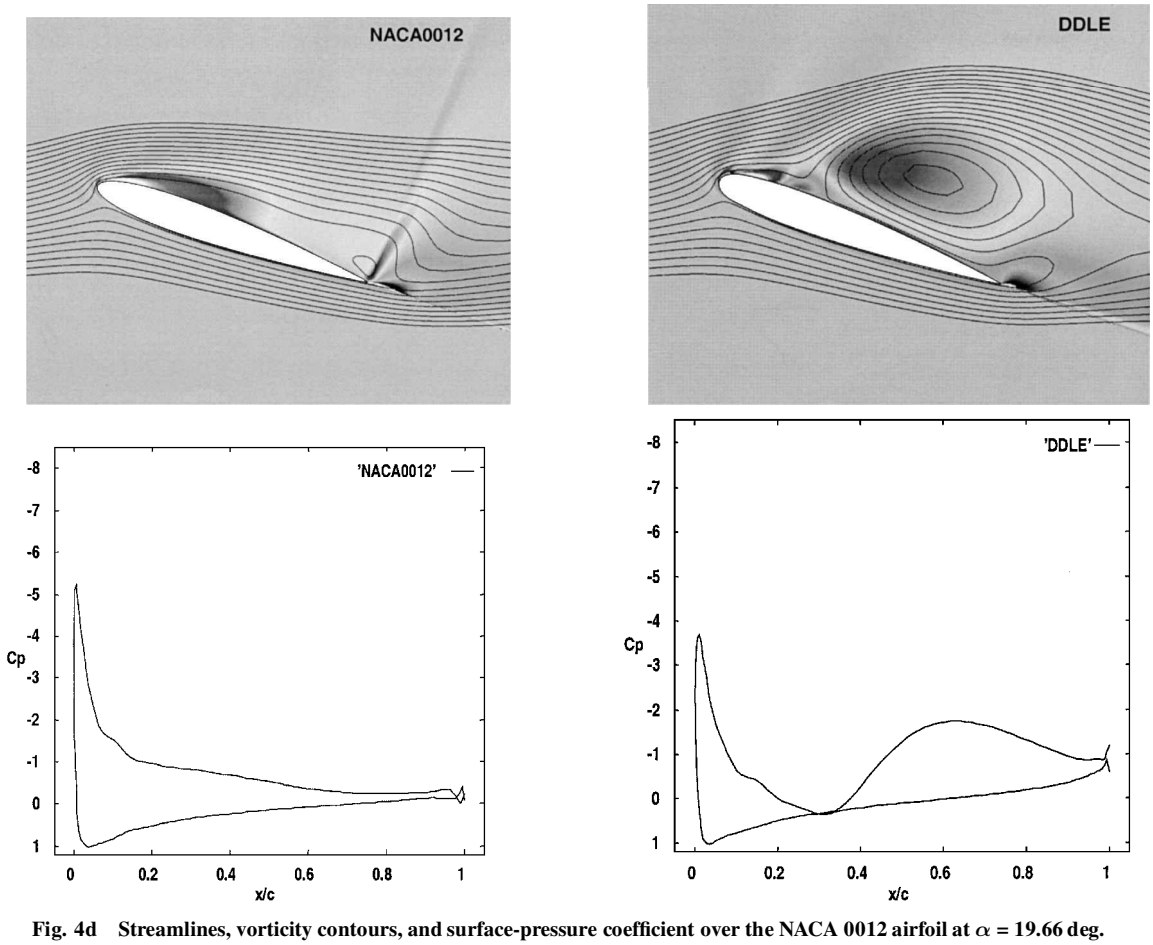

Fig. 4d Streamlines, vorticity contours, and surface-pressure coefficient over the NACA 0012 airfoil at α = 19.66 deg.

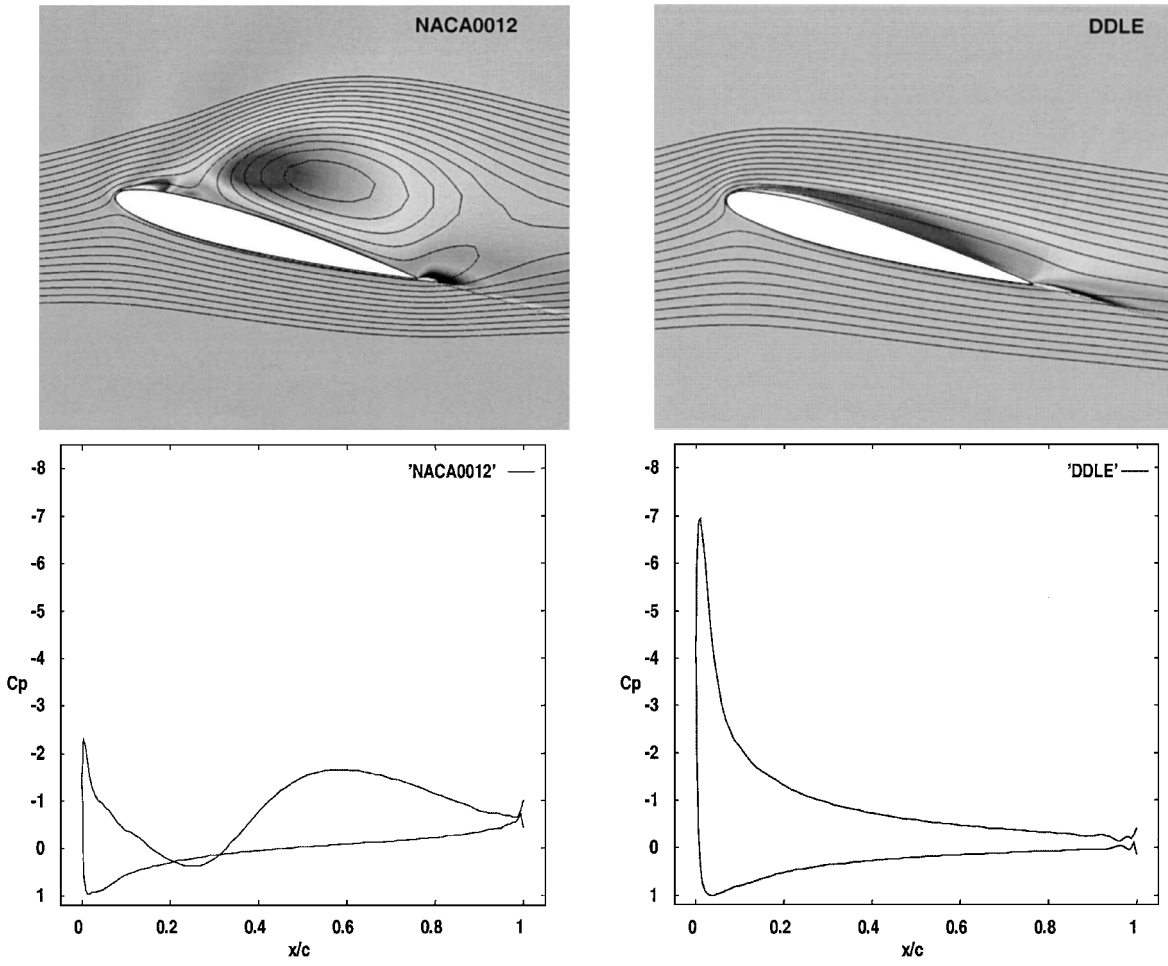

Fig. 4e Streamlines, vorticity contours, and surface-pressure coefficient over the NACA 0012 airfoil at α = 15.31 deg.

$$\Delta x_{i,j}^{n+1} = \frac{\sum k_{m,k} \Delta x_{m,k}^{n}}{\sum k_{m,k}} \tag{2a}$$

$$\Delta y_{i,j}^{n+1} = \frac{\sum k_{m,k} \Delta y_{m,k}^{n}}{\sum k_{m,k}} \tag{2b}$$

where the subscripts m, k indicate the grid points that are connected to point i, j. The new location of the interior nodes is determined by

$$x_{i,j}^{n+1} = x_{i,j}^{n} + \Delta x_{i,j}^{n+1} \tag{3a}$$

$$y_{i,j}^{n+1} = y_{i,j}^{n} + \Delta y_{i,j}^{n+1} \tag{3b}$$

Figure 1 shows the leading-edge shapes used. Figure 2 shows the amplitude of deformation as a function of time. The angle of attack of the airfoil is also shown. Figure 3 shows the body-fitted grid in the vicinity of the leading edge at several time levels. Good clustering of the grid and near orthogonality are evident.

Results and Discussion

Dynamic stall calculations were done for the baseline airfoil and the DDLE airfoil. The reduced frequency $k = \omega c/2V_\infty$ is 0.05, where ω is the circular frequency, c the airfoil chord, and V_∞ the freestream velocity. The airfoil pitching motion is described by $\alpha = 10^\circ + 10^\circ \cos(\omega t)$.

Four sets of calculations were done: 1) NACA 0012 airfoil at a freestream Mach number $M_\infty = 0.3$; 2) DDLE airfoil at $M_\infty = 0.3$, with the variation shape described in Ref. 7; 3) the DDLE airfoil with a fixed "thickest" shape at $M_\infty = 0.3$; and 4) DDLE airfoil at $M_\infty = 0.4$. The Reynolds number in all of these cases was 1.065×10^6.

The present preliminary calculations assume that the flow is turbulent everywhere. At the Reynolds number of the experiment, there is a large laminar region present, and the transition point moves with the angle of attack. The transition location dramatically affects the onset of separation, and ultimately, the stall. A sophisticated transition model is required to be developed for pressure gradient flows for use here. In its absence a one-to-one comparison between the present theory and experiments is not possible at this time. Nevertheless, the qualitative differences between the NACA 0012 and the DDLE airfoil behavior are in accord with what was observed in the experiments.

NACA 0012 vs DDLE Airfoil

Figure 4 shows the streamlines, and the vorticity contours around the oscillating NACA 0012 and the DDLE airfoils at selected instances in time. The surface-pressure distribution is also shown at these time levels. During the upstroke, up to an angle of attack of 18 deg or so, the flowfield remains attached over both the airfoils. Some increased thickening of the boundary layer is evident on the upper surface as the angle of attack increases.

Around 19.43 deg during the upstroke, the NACA 0012 airfoil develops a strong leading-edge vortex, seen as a "bump" in the surface-pressure distribution in Fig. 4b. The streamlines show considerable amount of separation and recirculation on the upper surface. In contrast, for the DDLE airfoil even though the entire upper surface boundary layer has separated the thickness of the separation bubble is smaller. There is also no evidence of a leading-edge vortex in the vorticity contours or the surface-pressure distribution.

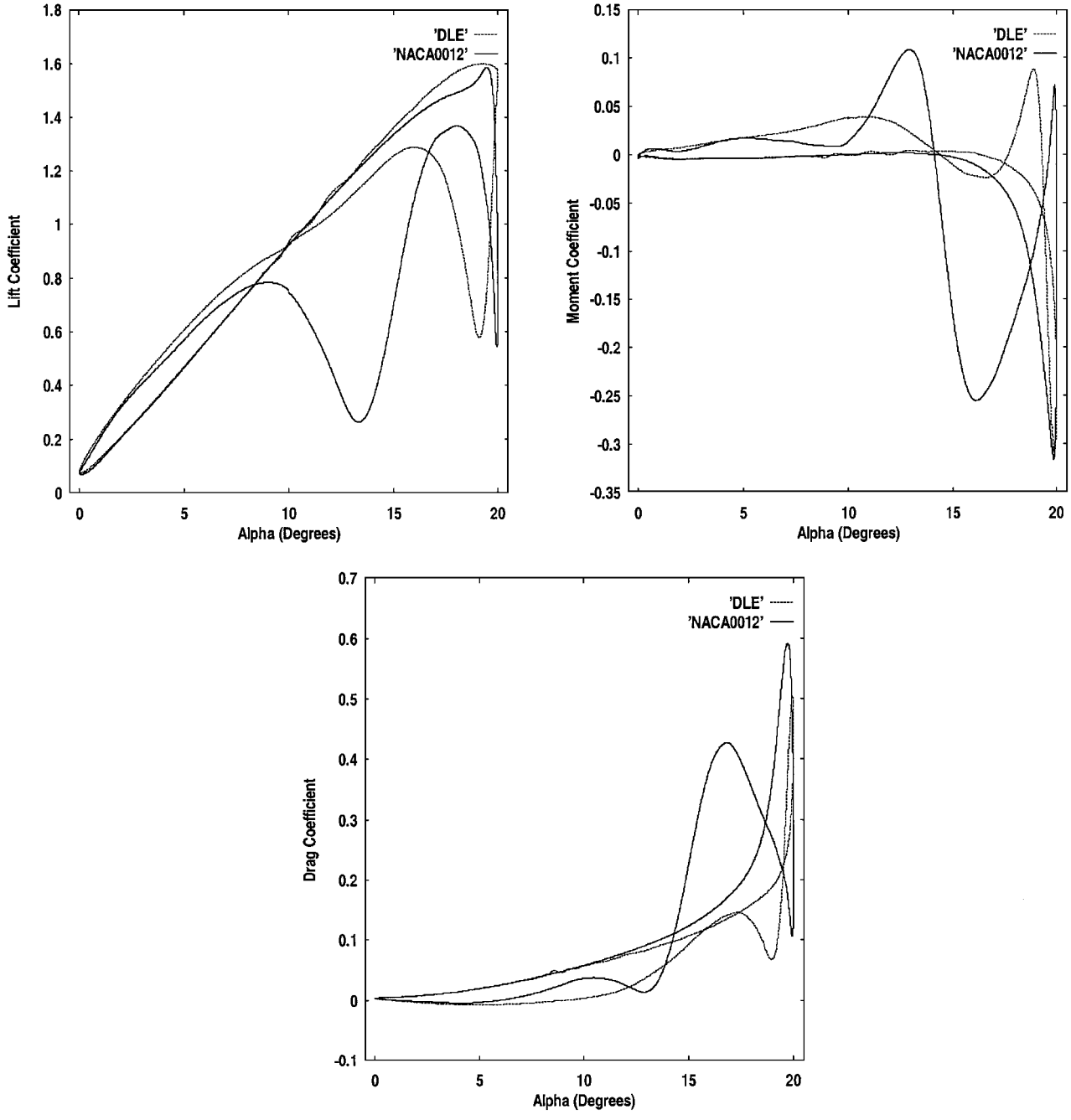

Fig. 5 Lift, drag, and pitching-moment hysteresis loops for the NACA 0012 and the DDLE airfoils.

At the end of the upper stroke, at $\alpha = 20$ deg the streamline plot and the vorticty contours both indicate that leading-edge vortex has already been shed for the NACA 0012 airfoil. There is a considerable loss in lift, as evidenced by the collapse of the suction peak. The DDLE airfoil, in contrast, is just beginning the dynamic stall process. It thus appears that the dynamic stall process is delayed by half a degree or so, as a result of the deforming leading-edge action.

During the downstroke, as shown by the pressure, vorticity, and streamline plots at $\alpha = 19.66, 15.31$ deg, the flow over the NACA 0012 airfoil and that over the DDLE airfoil are completely different. A second vortex forms and sheds over the NACA 0012 airfoil. The DDLE airfoil, on the other hand, experiences a gradual attachment of the boundary layer with the separation point migrating from the leading edge to the trailing edge. It thus appears that the DDLE action dramatically improves the airfoil performance during the downstroke. By the time the airfoil reaches an angle of attack of 10 deg, the flowfield has attached and is well behaved for both the airfoils.

Figure 5 shows the load hysteresis loops for the DDLE airfoil and the baseline NACA 0012 airfoil. As expected, for the NACA 0012 airfoil the lift drops abruptly twice during the downstroke. The pitching-moment distribution also shows two large negative peaks attributable to the large levels of suction that develop near the airfoil trailing edge as the vortex moves over the airfoil. The DDLE airfoil, on the other hand, shows just a single drop in the lift and a single peak in the pitching moment. These abrupt variations in the lift and pitching moment directly translate into vibratory loads on the fuselage and contribute to pitch link fatigue. It is clear that the DDLE airfoil is preferred over the NACA 0012 airfoil from these two (vibratory load and fatigue) considerations.

DDLE Airfoil with a Fixed Shape

Given the benefits of the DDLE airfoil, the following question arises. How much of the benefit is attributable to the changes to the shape, and how much is attributable to the surface dynamics, i.e., the rate of change of slope? To answer this question, the DDLE

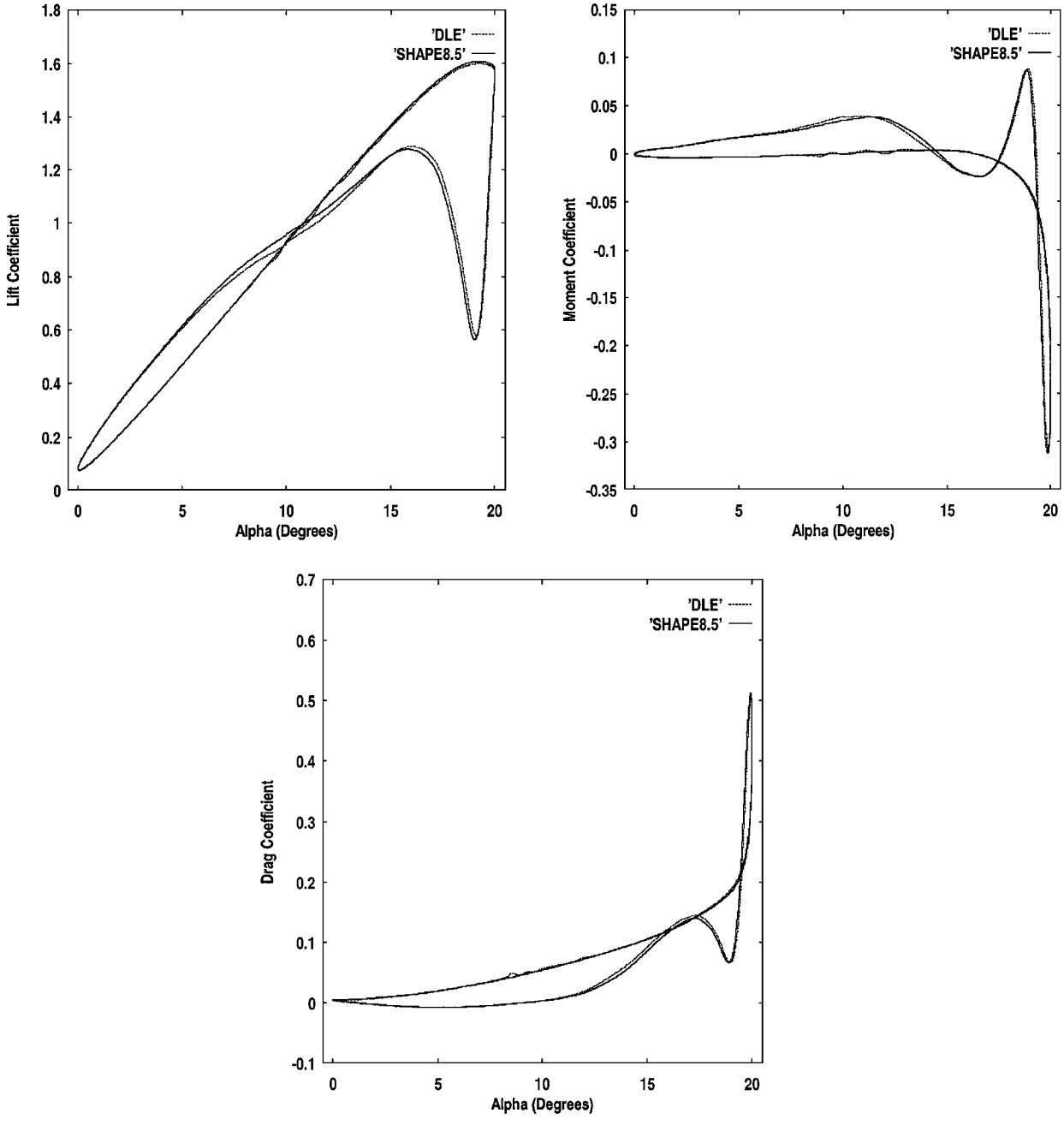

Fig. 6 Comparison of the load hysteresis characteristics between the DDLE airfoil and the fixed 8.5 shape.

dynamics stall calculations were repeated, with a fixed shape that corresponds to "shape 8.5" in Ref. 6. This corresponds to the largest leading-edge radius and the bluntest leading edge. It was found that the streamline, vorticity contour, and surface-pressure variations with angle-of-attack behavior were identical to the DDLE shape. The integrated loads, as shown in Fig. 6, were identical for the DDLE shape (where the airfoil shape continually changes) and the fixed 8.5 shape.

Thus it appears that much of the benefits of the DDLE airfoil were attributable to just the increased leading-edge radius and not the rate of change. A passive well-designed shape should be able to experience a milder dynamic stall for the conditions studied, rather than the NACA 0012 airfoil.

On the other hand, a blunter, thicker passive airfoil shape may have undesirable high-speed characteristics. The blunter leading edge can lead to high locally supersonic velocities and premature formation of shocks on the advancing side. The DDLE shape is thus a compromise between the baseline airfoil that may have good high-speed characteristics and a thicker, blunter airfoil that has good dynamic stall characteristics.

Behavior of the DDLE Airfoil at Higher Mach Numbers

To determine the behavior of the DDLE airfoil (with a dynamically changing shape) at higher Mach numbers, the preceding calculations were repeated at $M_\infty = 0.4$. From a visualization of the streamline and vorticity contours (not shown here, for brevity), the following phenomena were observed. The flow separated immediately downstream of the shock wave. During the upstroke, around 15 deg or so, a weak shock formed on the upper surface. The shock-induced separation process and the gradual upstream migration of the turbulent flow separation point combined to trigger a dynamic stall event during the upstroke. The flow attempted to recover during the downstroke, but a second vortex quickly formed and shed. The lift, drag, and pitching-moment variations are shown

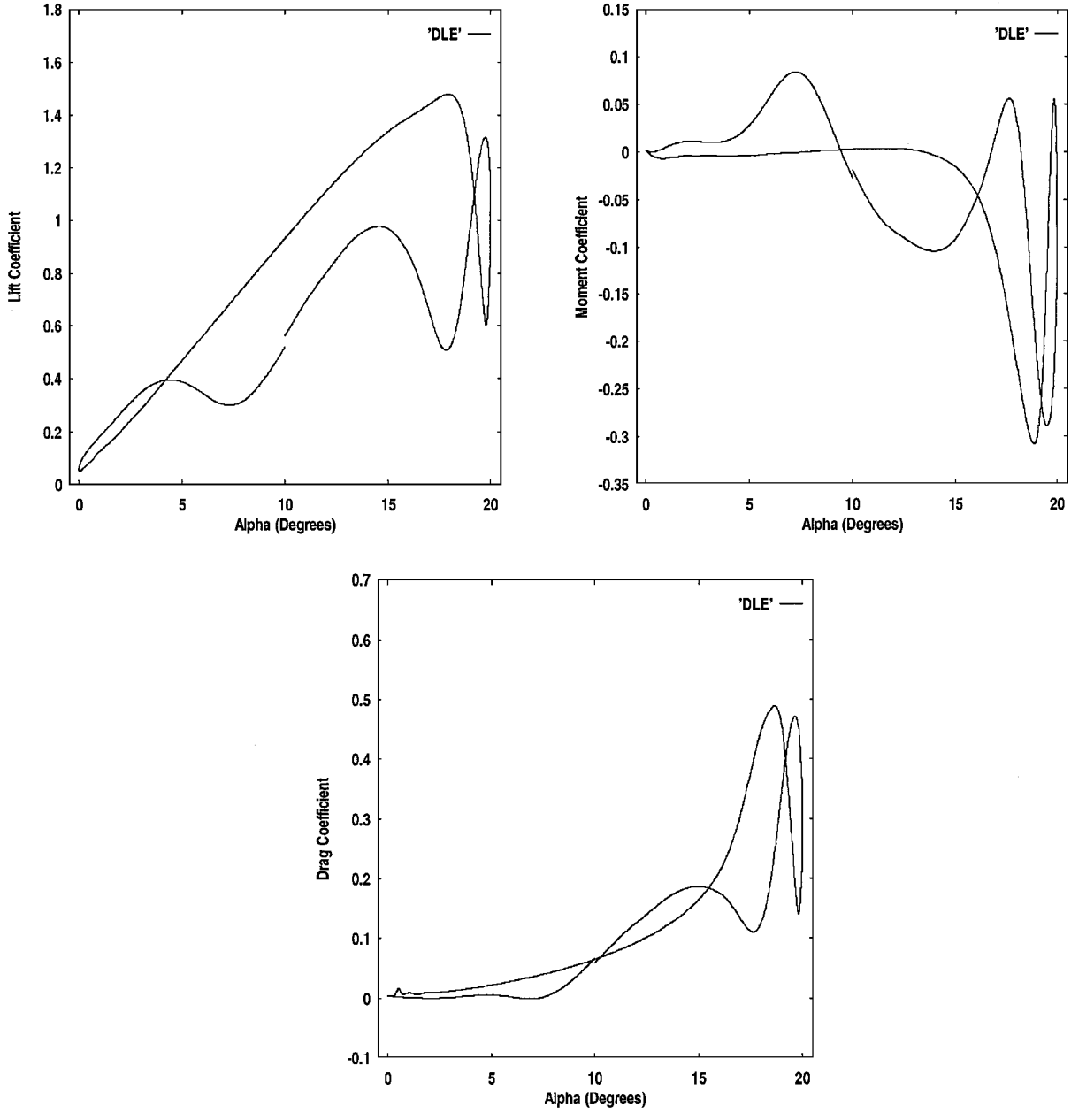

Fig. 7 Dynamic stall load hysteresis characteristics of the DDLE airfoil at $M_\infty = 0.4$.

in Fig. 7. It appears that the DDLE airfoil, with the surface shape variation schedule given in Ref. 6, was not effective in mitigating the dynamic stall process at this higher Mach number. Additional studies are needed to arrive at DDLE shapes that behave well at higher Mach numbers.

Conclusions

The preliminary results of dynamic stall calculations have been presented for both NACA 0012 and DDLE airfoils at two Mach numbers: 0.3 and 0.4. At the lower Mach number it was found that the DDLE airfoil had better dynamic stall characteristics over a conventional NACA 0012 airfoil. The numerical calculations showed that this improvement was caused by shape itself, not the rate at which the shape was changed. Therefore the shape 8.5 airfoil can be as effective as the DDLE airfoil. However for the rotary-wing aircraft applications the fixed-shape airfoil may experience a shock-induced stall over the advancing rotor blade. At the higher Mach number, the DDLE shape experienced a shock-induced stall during the upstroke, and its dynamic stall characteristics were quite similar to that of the NACA 0012 airfoil at low Mach numbers. Additional both numerical and experimental studies are needed to develop deforming leading-edge shapes that perform satisfactorily at high Mach numbers.

These preliminary results are in qualitative agreement with the experiment. However, because the flow in the experimental study was transitional in nature, the peak suction developed was smaller than found in the present study. Further, both the shape 8.5 airfoil and the DDLE airfoil flows were dynamic stall vortex free. A complete modeling of the transition behavior of the flow may enable better agreement between the present theory and experiments.

References

[1]Carr, L. W., McAlister, K. W., and McCroskey, W. J., "Analysis of the Development of Dynamic Stall Based on Oscillating Airfoil Experiments," NASA TN-D-838270, 1977.

[2]Carr, L. W., and McAlister, K. W., "The Effects of Leading Edge Slat on the Dynamic Stall of an Oscillating Airfoil," AIAA Paper 85-2533, Oct. 1983.

[3]Tuncer, I., and Sankar, L. N., "Unsteady Aerodynamic Characteristics of a Dual-Element Airfoil," *Journal of Aircraft*, Vol. 31, No. 3, 1994, pp. 531–537.

[4]Bangalore, A., and Sankar, L. N., "Numerical Analysis of Aerodynamic Performance of Rotors with Leading Edge Slats," *Journal of Computational Mechanics*, Vol. 17, No. 5, March 1996, pp. 335–342.

[5]Seifert, A., Bachar, T., Koss, D., Shepshelovich, M., and Wygnanski, I., "Oscillatory Blowing—A Tool to Delay Boundary Layer Separation," *AIAA Journal*, Vol. 31, No. 11, 1993, pp. 2052–2060.

[6]Hassan, A. A., "Applications of Zero-Net-Mas Jets for Enhanced Rotorcraft Aerodynamic Performance," *Journal of Aircraft*, Vol. 38, No. 3, 2001, pp. 478–485.

[7]Chandrasekhara, M. S., Wilder, M. C., and Carr, L. W., "Unsteady Stall Control Using Dynamically Deforming Airfoils," *AIAA Journal*, Vol. 36, No. 10, 1998, pp. 1792–1800.

[8]Wu, J. C., Huff, D. L., and Sankar, L. N., "Evaluation of Three Turbulence Models in Static Airloads and Dynamic Stall Predictions," *Journal of Aircraft*, Vol. 27, No. 4, 1990, pp. 382–384.

[9]Sankar, L. N., Malone, J. B., and Schuster, D., "Euler Solutions for Transonic Flow Past a Fighter Wing," *Journal of Aircraft*, Vol. 24, No. 1, 1987, pp. 10–16.

[10]Bangalore, A., and Sankar, L. N., "Forward Flight Analysis of Slatted Rotors Using Navier–Stokes Methods," *Journal of Aircraft*, Vol. 34, No. 1, 1997, pp. 80–86.

[11]Chang, I.-C., Torres, F. J., and Tung, C., "Geometric Analysis of Wing Sections," NASA TM-110346, 1995.

[12]Batina, J. T., "Unsteady Euler Airfoil Solutions Using Unstructured Dynamic Meshes," *AIAA Journal*, Vol. 28, No. 8, 1990, pp. 1381–1388.